Deformation and Plasticity of Materials under Extreme Conditions

Sébastien Merkel

Deformation and plasticity of materials under extreme conditions

Sébastien Merkel

Univ. Lille, CNRS, INRAE, ENSCL, UMR 8207 - UMET - Unité Matériaux et Transformations, F-59000 Lille, France

Abstract

Understanding mechanical properties and their microscopic origins is fundamental for multiple fields in condensed matter research. They are controlled by defects, dislocations, diffusion, as well as microstructures, which are not trivial to study under extreme conditions. This chapter summarizes the last 25 years of advances in high pressure devices, x-ray measurements, and data interpretation capabilities for addressing the deformation and plasticity of materials under extreme conditions, from experiments in large volume presses or diamond anvil cells, texture and stress analysis in powder x-ray diffraction, multi-grain crystallography, to self consistent models of materials behavior. Examples of applications are then provided in the fields of geophysics and materials science along with perspectives for studies of plastic deformation under extreme conditions in the coming years.

1 Introduction

Mechanical properties are important for a range of applications, from the design of materials with advanced properties to the dynamics of planetary interiors. The plastic behavior of solid is controlled by defects, dislocations, diffusion, as well as microstructures, a generic term describing the arrangement of a material from the nm to the cm scale. Microstructures in minerals, for instance, are important for the dynamics of the deeper layers of the Earth (Karato et al. 2000). For such application, materials of interest include the high pressure phase of Fe, ε-Fe (Wenk et al. 2000, Lincot et al. 2016), bridgmanite and ferropericlase (Miyagi and Wenk 2016, Marquardt and Miyagi 2015, Girard et al. 2016, Nzogang et al. 2018), or post-perovskite (Merkel et al. 2007, Miyagi et al. 2010, Dobson et al. 2013), most of which are not stable under ambient pressure and temperature and should be studied *in-situ*. Hydrostatic pressure also induces phase transformations in metals. Titanium and zirconium, for instance, are hexagonal-close-packed metals under ambient conditions. Under high pressure, they transform to another hexagonal structure, the ω phase, which is not compact and for which mechanical properties are poorly constrained (Yu et al. 2015, Wenk et al. 2013, Kumar et al. 2020). In other cases, high pressure has been used as a fine-tuning parameter for optimizing strength and grain sizes (e.g. Zhou et al. 2020). As such, the study of mechanical properties in-situ under extreme conditions is of general interest.

The last 25 years have seen tremendous advances in high pressure instruments coupled with synchrotron radiation that allow studies of microstructures and mechanical properties under high pressure and high temperature (Raterron and Merkel 2009). The group at the Geophysical Laboratory and H.-K. Mao

provided key contributions to this field, through the design of new methods and ground-breaking publications (e.g. Hemley et al. 1997, Mao et al. 1998, Wenk et al. 2000, Merkel et al. 2002). Nowadays, millimeter size samples are deformed in *large volume presses* (LVP) up to Earth's uppermost lower mantle pressures. High pressures and lower dimension samples are deformed and studied in *diamond anvil cells* (DAC). In all cases, samples are submitted to a macroscopic deformation to induce plasticity and deformation microstructures. Their properties are then studied *in-situ* using X-ray diffraction and imaging. X-ray radiography allows the measurement of macroscopic properties, such sample size and the applied macroscopic deformation. X-ray diffraction on polycrystals allows for extracting average sample properties by the study of lattice preferred orientations (LPO) and the average stress state. Multigrain X-ray diffraction (sometimes labeled as 3D-XRD) addresses single-grains inside a polycrystalline matrix and, in some cases, allows for measuring densities of defects such as dislocations. As such, the properties of deforming materials can be studied *in-situ*, in their stability field or conditions of application.

In this chapter, I will present the experimental techniques for the high pressure study of materials plasticity. I will start with a description of the experimental devices, then present the characterization techniques using in-situ X-rays, modeling using self-consistent calculations, sample results for Earth's and other materials, and perspectives for the years to come.

2 Experimental techniques

2.1 Plasticity in the large volume press

The Deformation-DIA (D-DIA), Rotational Drickamer (RDA), and deformation T-Cup (D-Tcup) are the main LVP for deformation experiments coupled with *in-situ* characterization under high pressure. All allow the controlled deformation of millimeter size samples. In addition, new apparatuses such as the RoToPEc (rotational tomographic Paris Edinburgh cell) and high-pressure X-ray tomography microscope (HPXTM) are devices under development.

The D-DIA (Wang et al. 2003, Fig. 1) is a hydraulic press in which a cubic assembly is deformed under the action of 6 anvils. Heating sleeves allow temperatures up to ≈2000 K. Hydrostatic compression is obtained by advancing all 6 anvils (4 horizontal and 2 vertical) at the same velocity. Axial compression deformation at constant pressure is obtained by advancing the upper anvils while retracting the horizontal anvils. Lateral compression is obtained by retracting the vertical anvils and advancing the horizontal anvils. The D-DIA allows experiments at strain rates ranging from 10^{-7} to 10^{-2} s^{-1} and pressures and temperatures up to 18 GPa and 1900 K (Kawazoe et al. 2013). It has also been adapted for deformation using a shear geometry up to 25 GPa and 1873 K (e.g. Fig 2a, Tsujino et al. 2016, Nishihara et al. 2018). Work is underway to develop new generations of D-DIA-like presses such as the D-DIA-30 allowing reaching higher pressures and working on larger samples (e.g. Wang and Shen, 2014). The D-TCup (Hunt et al. 2014, Hunt and Dobson 2017) is a similar setup with second stage anvils being developed to allow deformation experiments at pressures and temperatures exceeding those of the D-DIA. In all cases,

the imposed macroscopic strain of the cell assembly is axial and measured *in-situ* using X-ray radiography (see below). Lateral macroscopic strain is reconstructed based on the axial macroscopic strain and the sample's change of volume, deduced from x-ray diffraction.

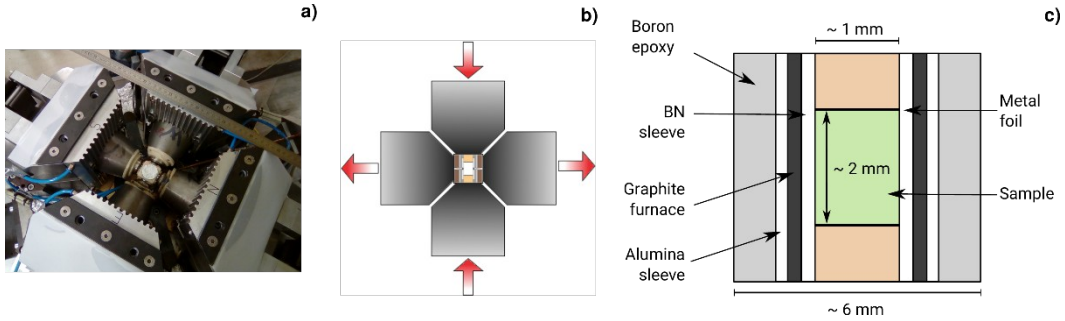

Figure 1: (a) Main module of the D-DIA deformation press at the ID06 beamline of the ESRF synchrotron. The main anvils, labeled as here E, W, N, and S, apply a load on secondary anvils to generate deformation. The lower (hidden) and top (opened) anvils are not visible on the image. (b) Principle of the D-DIA. Vertical and horizontal anvils can be moved independently. (c) Typical sample assembly placed between the 6 anvils for deformation experiments. For simplicity, the thermocouples measuring temperature are not shown.

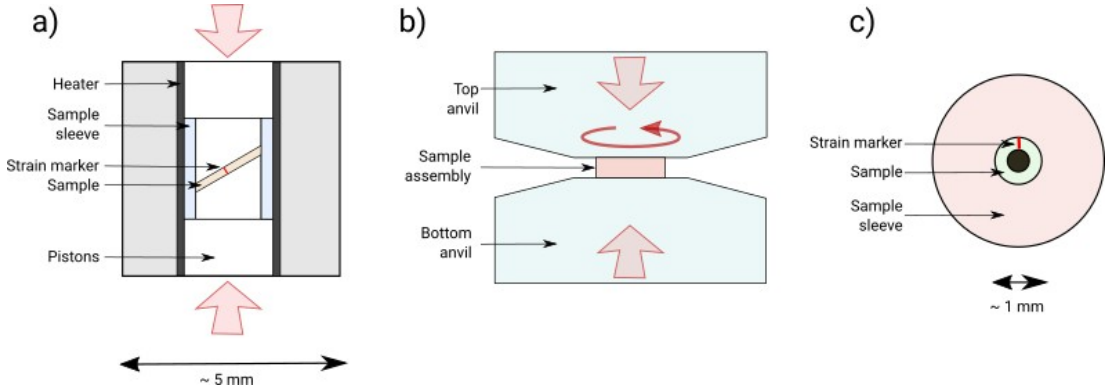

Figure 2: Typical sample assemblies for shear deformation in the LVP. (a) Shear deformation in the D-DIA (e.g. Tsujino et al. 2016). Axial strain (red arrows) is applied to the cell assembly, which translates to shear strain on the sample. (b) Torsion in the RDA. Pressure is applied by advancing the top and bottom anvils. The cell assembly is submitted to torsion by rotating one of the anvils. (c) Simplified top view of the cell assembly in the RDA in Girard et al. 2016. The sample is a ring of 0.2 mm thickness, 0.45 mm inner diameter and 1 mm outer diameter.

The rotational Drickamer (RDA, Fig. 2b) is an opposed anvil high pressure device that has been modified to perform large strain deformation experiments in simple shear geometry (Yamazaki and Karato 2001).Samples can be sheared between two anvils under pressure by a rotation actuator, with strains exceeding $\gamma \approx 6$ at high pressure at strain rates similar to those of the D-DIA. Early sample designs used disks of less that 0.8 mm thick and up to 4 mm outer diameter (e.g. Yamazaki and Karato 2001) while recent experiments rely on rings of 0.2 mm thickness, 0.45 mm inner diameter and 1 mm outer diameter

3

for a better control of sample strain (Fig 2c, Girard et al, 2016). The RDA was successfully used to obtain quantitative creep results on wadsleyite (Nishihara et al. 2008, Kawazoe et al. 2010, Farla et al. 2015), ringwoodite (Miyagi et al. 2014), and bridgmanite and magnesiowüstite aggregates (Girard et al. 2016) up to 27 GPa and 2150 K. In the RDA, the stress applied to the sample is evaluated using x-ray diffraction and is a combination of pure shear and axial compression (Xu et al. 2005).

New advances in the field also include the coupling deformation in simple shear using torsion devices such as the RoToPEc and HPXTM with tomographic measurements. Proofs of principles have been published (Philippe et al. 2016, Wang et al, 2011) and the devices are currently in use at synchrotron sources.

2.2 Plasticity in diamond anvil cells

Large volume presses allow controlled deformation at constant pressure and temperature but do not cover the entire range of conditions found in the Earth's interior. DAC, on the other hand, allow static experiments at pressures exceeding that at the center of the Earth (Dewaele et al. 2018) and combined pressures and temperatures of the Earth's core (Tateno et al. 2010). In addition to confining pressure, diamonds in the DAC impose an axial compressive stress. In most experiments, the compressive stress is reduced by using pressure media around the sample. In plasticity studies, this comes at a benefit that allows macroscopic deformation of the sample. Unlike deformation in LVP, however, pressure and deformation can not be decoupled. Deformation experiments in the DAC are not performed at constant pressure nor at controlled stress or strain rates. The total plastic strain in DAC experiments, estimated from the magnitude of texture evolution, is on the order of 10 to 30%. It is applied over a duration of 5 minutes to a few hours, translating to a strain rate estimate ranging from 10^{-5} to 10^{-3} s^{-1}.

In most DAC experiments, the sample properties are studied through the diamond anvils which are transparent over a broad range of wavelength, including X-rays (Fig. 3a). For plasticity studies, it can be useful to have the incoming x-ray beam perpendicular to the loading axis (Fig. 3b). In the early radial diffraction experiments, the sample itself served as a gasket material (Kinsland and Bassett 1977). The sample stress state however, was complex with large pressure gradients across the sample. The technique was then improved by the group at the Geophysical Laboratory with the use of beryllium gaskets (Hemley et al. 1997) for a better controlled sample pressure and stress state, and further improved with the use of amorphous boron / epoxy composite gaskets (Merkel and Yagi 2005). Early radial x-ray diffraction experiments were performed at ambient temperature (Hemley et al. 1997, Mao et al. 1998, Wenk et al. 2000, Merkel et al. 2002).

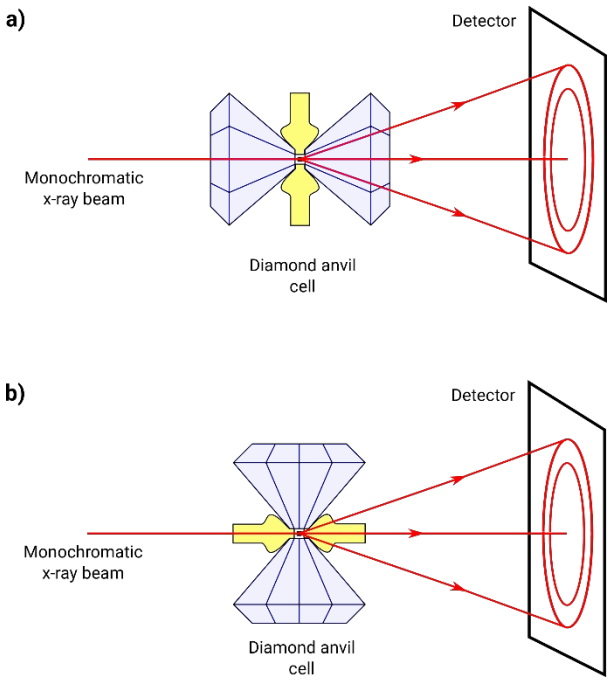

Figure 3: Geometries for x-ray diffraction DAC experiments. The axial geometry (a) is most common, with the incident x-ray beam aligned with the compression direction. The radial geometry (b) is commonly used in deformation experiments. The incoming and diffracted x-ray beams are perpendicular to compression, and pass through an x-ray transparent gaskets made of beryllium or composite materials.

High temperature deformation studies have been attempted by combining laser heating and diffraction in the radial geometry, with limited success due to large temperature gradients in the sample (Miyagi et al. 2008). In order to obtain homogeneous conditions of stress, pressure, and temperature, efforts were hence invested in developing dedicated DAC systems combined with resistive heating allowing for radial x-ray diffraction (Liermann et al. 2009, Immoor et al. 2020), sometimes also complemented with additional laser-heating (Miyagi et al. 2013). Under ambient temperature, radial diffraction experiments reached pressures of nearly 300 GPa (Hemley et al. 1997). Combined conditions of 62 GPa at 1400 K were obtained in the resistive heating setup (Immoor et al. 2018) and 69 GPa at 2273 K for setups combining laser and resistive heating (Miyagi et al, 2013).

In addition, deformation experiments can be performed using a rotational diamond anvil cell (rDAC). In the rDAC, one of the diamond anvils is allowed to rotate which produces a torsional deformation like in the RDA (Blank et al. 1984). The rDAC has the potential to achieve large-strain under ultra-high pressure conditions while attaining a steady-state deformation (Levitas 2004, Nomura et al. 2017). To this day, however, the use of the rDAC for true deformation experiments has been limited due to the complex stress and strain field in rDAC experiments (Ma et al. 2006, Zarechnyy et al. 2012). The reliability of rDAC experiments is being improved, with new anvil designs for slip-free experiments which could considerably improve the usability of the technique (Azuma et al. 2017).

5

2.3 Computational plasticity

Experimental techniques can be limited. In particular, when addressing the plastic properties of minerals in planetary interiors, experiments are performed at strain rates that are orders of magnitude above those of nature. As such, numerical approaches can become useful to understand, model, and extrapolate materials behavior.

Plastic deformation is the results of the complex, collective behavior of a large collection of defects within a material microstructure. Until recently, this task was not within the reach of numerical techniques but recent developments open the door to such studies (e.g. Cordier et al. 2012, Boioli et al. 2017, Reali et al. 2019). Such methods go beyond the scope of the current chapter but a detailed description can be found in Cordier and Goryaeva (2018).

3 In situ caracterization techniques

3.1 Deformation

In LVPs, the sample's macroscopic deformation is measured using X-ray radiography. Strongly x-ray absorbing samples are visible directly while, for less-absorbing samples, one places foils of gold, platinum, or molybdenum in the sample assembly (e.g. Fig. 1c). Based on the displacement, shortening, or tilting of the metal makers, one can then reconstruct the macroscopic deformation applied to the sample (e.g. Raterron and Merkel 2009, Farla et al. 2015). Strain vs. time plots are then used to evaluate the sample strain rate.

In DACs, deformation is rarely controlled and occurs during pressure increases. Moreover, the sample thickness is on the order of 20 μm. Decent sample images can be obtained using changes in X-ray transmission contrasts (Merkel and Yagi 2005) but deformation are not very well resolved and, hence, these are rarely used. This could be improved using phase contrast imaging (e.g. Schropp et al. 2015) which allows for a much better resolved imaging of interfaces, and particularly so at upgraded synchrotron sources such as ESRF-EBS with an improved performance by a factor of 100 in beam coherence. To my knowledge, this has not been attempted yet.

3.2 Polycrystal properties

Powder x-ray diffraction is a standard technique for assessing average macroscopic sample properties, and can be applied to both DAC and LVP experiments. The diameter of the incident x-ray beam and sample microstructures, however, should be adjusted so that a statistically relevant number of grains contribute to the diffraction signal. Otherwise, statistical assumptions with the powder x-ray diffraction processing methods will fail and may lead to inconsistent results.

3.2.1 Lattice preferred orientations

Often, crystallites in a polycrystal are not randomly distributed in orientation and materials develop *lattice preferred orientations* (LPO). LPO can arise from processes such as nucleation, phase transformation, or plastic deformation. LPO have a strong influence on mechanical properties as physical properties become anisotropic (Kocks et al. 1998). They also affect the propagation of seismic waves and are hence of great interest in geosciences (Mainprice et al. 2000).

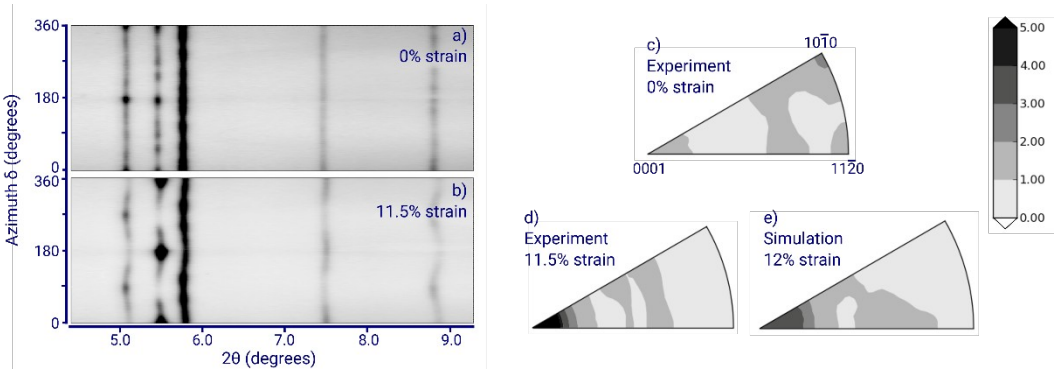

Figure 4: Diffraction images for ε-Fe at 17 GPa and 400 K (Merkel et al. 2012) measured at the start of the deformation (a) and after 11.5% axial strain in a D-DIA (b). Variations of peak intensities and positions with azimuth are indicative of the sample LPO and stress, respectively. Measured inverse pole figure of the compression direction at the start of deformation (c) and after 11.5% axial strain (d). (e) Results of a self-consistent model after 12% axial strain reproducing the measured sample strain and textures and constraining the strength of basal, prismastic and pyramidal slip as well as tensile twinning in ε-Fe at those conditions.

In high pressure deformation experiment, LPO measurements are often used to constrain plastic deformation mechanisms (Wenk et al. 2006). In fact, plastic deformation mechanisms and, in particular, dislocation glide will give rise to specific LPO in a polycrystals. LPO measurements, combined with texture modeling (see below) allow the identification of the active plastic deformation mode in a material.

Sample LPO appear as variation of diffraction intensities with orientation (Fig. 4) and can be extracted from the diffraction images using either Multifit (Merkel and Hilairet 2015) and BEARTEX (Wenk et al. 1998) or MAUD (Lutterotti et al. 1999, Wenk et al. 2014).

3.2.2 Stress and strains

Stress-strain and stress-pressure curves are a critical element to characterize the mechanical properties of materials. In-situ determination of stress, however, is not trivial in high pressure experiments. Unlike classical, low pressure, deformation experiments, the applied stress is not measured directly. Early publications estimated stress based on pressure gradients across a relatively large sample (e.g. Meade and Jeanloz, 1988), with the limitation that pressure and stress is heterogeneous in such sample, leading to discrepancies with other measurements (Reynard et al. 2019). Internal quartz calibrants can be used for in-situ piezometry in the DAC. Raman vibrational mode frequencies shift with pressure and deviatoric

7

stresses induce TO-LO splitting of the lowest frequency E mode of quartz. All have been calibrated recently (Reynard et al. 2019). Most high pressure deformation experiments, however, rely on in-situ x-ray diffraction for stress evaluation.

Residual stress analysis using x-ray diffraction is a common technique in materials science (Noyan and Cohen 1987) and was adapted to high pressure research in the mid-1990's (e.g. Hemley et al. 1997, Singh et al. 1998). Hydrostatic pressure changes the unit cell parameters of a material, and hence the average d-spacings of all powder x-ray diffraction lines. Deviatoric stresses add an additional component with changes of the measured d-spacings with orientation (Fig. 4a). Theories relating deviatoric stress and the measured strains using x-ray diffraction are available in the literature, both for axial (Singh et al. 1998) and shear (Nishihara et al. 2008) deformation experiments. All rely on elasticity theory and assume continuity of stress or strain within the deforming aggregate.

The elastic assumption for stress inversion, however, fails when plastic deformation is at play (Li et al. 2004, Merkel et al. 2006). In fact, as materials deform, stresses will relax in grains in soft orientations (i.e. for which plastic deformation can be easily activated) while other grains, whose orientations do not favor plastic deformation, will remain highly stressed. For each orientation, the measured d-spacing in powder x-ray diffraction is the average d-spacing of all grains contributing to the diffraction, either soft or hard. This heterogeneity of stress within grains contributing to the same diffraction peak is not well captured by elasticity-based models. The average stress state and intergranular stress heterogeneities in a deforming material, however, can be modeled using self-consistent techniques (see below, Fig. 7).

Another approach to circumvent the issue of stress evaluation using X-ray diffraction is to use an internal standard. Al_2O_3, for instance, is well-known and was calibrated using self-consistent techniques (Raterron et al 2013). Pyrope is another option as experiments have shown that it is plastically isotropic with less that 10 % variation for stresses deduced between different diffraction lines (e.g. Girard et al 2020).

3.2.3 Interpretation using self-consistent models

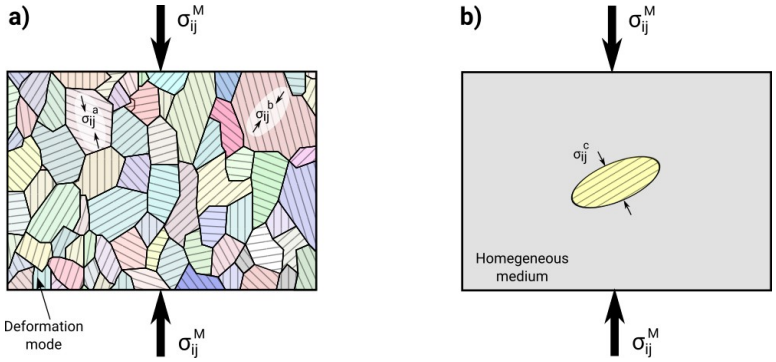

Figure 5: Polycrystalline simulation (after Amodeo et al. 2018). (a) In a polycrystal, stress and strain distributions are heterogeneous. The behavior of each grain depends on its local environment, elastic, and plastic properties. (b) In self-consistent models, each grain is treated as an elliptical inclusion inside a homogeneous medium.

Deformation experiment are best interpreted using self-consistent (SC) methods. SC calculations treat each grain of the polycrystal as an inclusion in a homogeneous but anisotropic medium (Fig. 5). The properties of the medium are determined by the average of all inclusions. At each deformation step, the inclusion and medium interact and the macroscopic properties are updated iteratively until the average strain and stress of all inclusions equals the macroscopic strain and stress.

The Elasto-Plastic Self-Consistent (EPSC) approximation of Turner and Tomé (1994), later extended by Clausen et al. (2008) and Neil et al. (2010), accounts for elasticity of the material as well as stress relaxation and grain rotation due to twinning and dislocation slip. Plasticity in EPSC calculations, however, is not dependent on strain rates. Visco-Plastic Self-Consistent (VPSC) calculations account for stress relaxation and grain rotation due to twinning and dislocation slip, accounting for a strain-rate dependent plasticity, but do not account for elasticity (Lebensohn and Tomé 1994). Finally, the Elasto-Visco-Plastic Self-Consistent (EVPSC) formulation, such as in Wang et al. (2010), accounts for elastic stresses, grain rotation, and relaxation due to plasticity, as well as strain rate dependence of the plastic behavior.

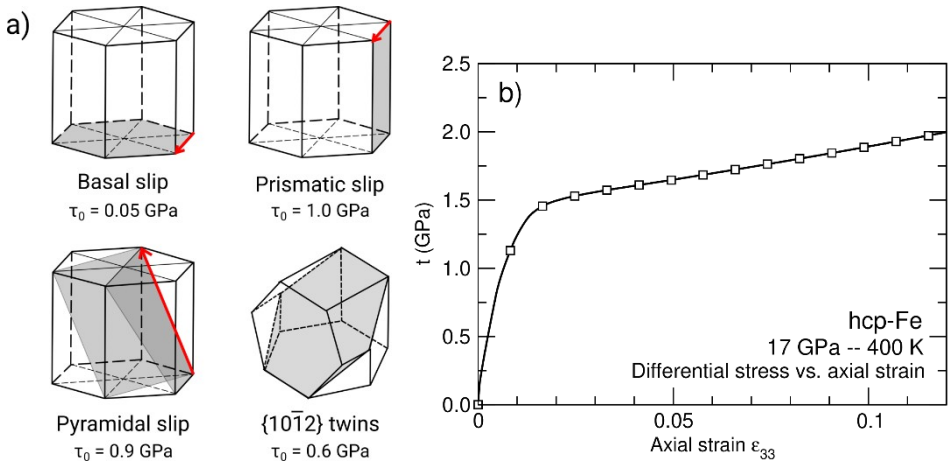

Figure 6: Plasticity of ε-Fe at 17 GPa and 400 K (after Merkel et al. 2012). (a) Dominant deformation mechanisms deduced from the data in Fig. 4. τ_0 is the initial CRSS, before hardening later in the deformation. (b) Differential stress vs. axial strain.

All SC calculations can be used to model the evolution of polycrystalline textures. Comparing the experimentally measured LPO and the results of SC calculations allows for the identification of dominant plastic deformation mechanisms and, in particular, dislocation slip or twinning. VPSC calculations, however, will not model macroscopic or intergranular stress, nor lattice strains measured in experiments. EPSC or EVPSC will allow interpreting both the experimental texture and lattice strains (Merkel et al. 2009, Lin et al. 2017, Li et al. 2004).

For ε-Fe at 17 GPa and 400 K, for instance, a comparison between experimental data and the results of EPSC models indicates that plastic deformation is dominated by the activity of basal slip and $\{10\bar{1}2\}$ tensile twinning (Fig. 6). The critical resolved shear stress (CRSS) of basal slip is low (0.05 GPa) but, due

9

to intergranular interactions and effects of grain orientations, the overall macroscopic stress reaches t=2.0 GPa after 12% axial compression.

Fig. 7 highlights one of the advantages on self-consistent models for analyzing the results of high pressure deformation experiments. Stresses deduced from elastic models are inconsistent due to stress heterogeneities between grains in soft orientations, for which stresses are relaxed through plastic deformation, and grains in hard orientations, which experience a higher stress. The results in an apparent stresses that can vary by up to 50% or more depending on the choice of measurement which will, later, translate into inconsistent flow laws. One should keep in mind, however, that x-ray diffraction is sensitive to strains at the local scale, for grains contributing to diffraction, and not stress. Self-consistent calculations (EVPSC in Fig. 7) allows determining the true stress value, consistent with all strain measurements using x-ray diffraction.

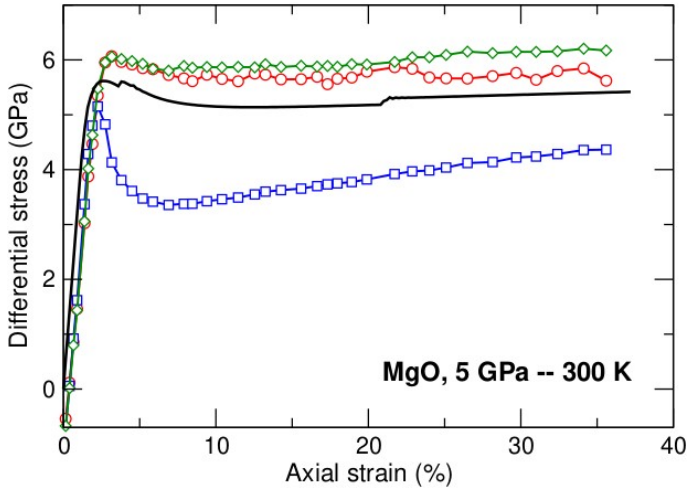

Figure 7: Stress in polycrystalline MgO plastically deformed at 5 GPa and 300 K in the D-DIA (Lin et al. 2017). The plot displays apparent stresses deduced from an elastic model and x-ray diffraction measurements on the 111, 200, and 220 diffraction lines. Solid back line is the result of EVPSC calculations. Plastic deformation results in different stress values in the elastic model, which is inconsistent: average stress in the polycrystal should be unique. This can be solved by modeling the experiment using self-consistent calculations.

3.3 Plasticity at the grain scale

Recently, experimental studies of microstructures and plastic deformation reached a new milestone with techniques allowing the characterization of individual grains or subgrains within a polycrystalline material (Ludwig et al. 2009). Multigrain x-ray diffraction allows for a rapid, in-situ, and non-destructive study of microstructural elements. These elements can also be followed in situ as a function of time or external parameters such as stress, pressure, or temperature. Moreover, samples in high pressure experiments and, in particular, those of DAC are often small and do not contain enough grains for a

statistically relevant powder diffraction analysis. They are, on the other hand, perfectly suited for multigrain x-ray diffraction.

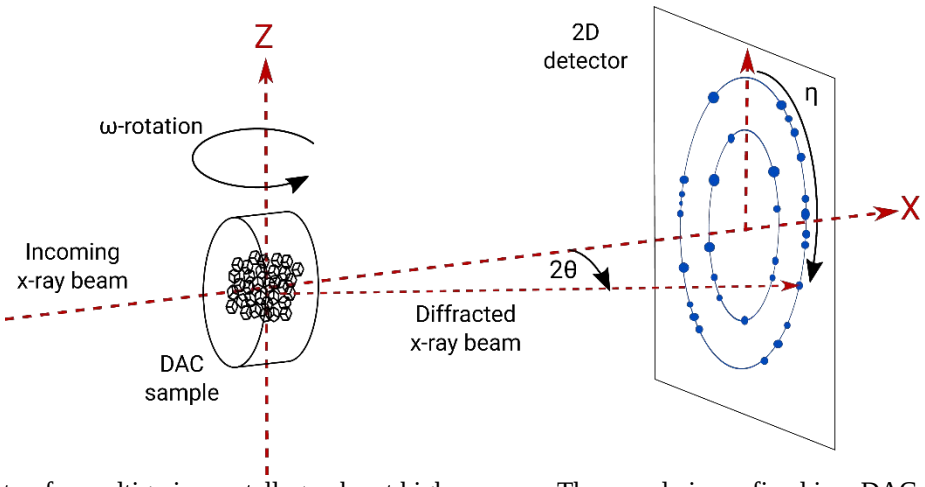

Figure 8: Setup for multigrain crystallography at high pressure. The sample is confined in a DAC in axial geometry with an ω rotation parallel to the Z direction. Diffraction patterns are collected on a flat panel detector orthogonal to the incoming X-ray beam over Δω ranges of ≈50° in steps of δω≈0.5°. Individual grains inside the polycrystalline sample give rise to diffraction spots at specific 2θ, ω, and η angles.

3.3.1 Multigrain crystallography

Multigrain x-ray diffraction allows for the extraction of the orientation and crystal structure of hundreds of elements inside a polycrystalline material (Poulsen 2004). Extensions of the technique further allow the determination of the position and stress state for each of those elements (Oddershede et al. 2010).

The method has been applied to DAC experiments (Nisr et al. 2012, Rosa et al. 2016, Zhang et al. 2014, Langrand et al. 2017) including pioneering works involving H.-K. Mao (Ice et al. 2005). The method is not restricted to DAC experiments and could also be applied to LVP experiment but this remains to be reported. Multigrain x-ray diffraction consists in a search for diffraction spots while exploring reciprocal space (Fig. 8). A first analysis generates a database of experimental diffraction spots, along with their 2θ, ω, and η angles and intensities. Algorithms such as GrainSpotter (Schmidt 2014) then use the experimental diffraction spots database and scan the grain orientation space to reconstruct the number and orientations of the individual diffracting sample grains.

In the work of Rosa et al. (2016), for instance, we used multigrain x-ray diffraction in order to study the effect of olivine-wadsleyite-ringwoodite chain of phase transformations on microstructures up to 22 GPa and 940 K. We follow the number of grains for each phase, their orientations, a distribution of grain sizes, at each step of the phase transformation (Fig. 9). Such measurement allow the study of phase transformation mechanisms and associated microstructures, with important applications for constraining deep-Earth processes. They can, as well, be extended to follow microstructures induced by plastic deformation.

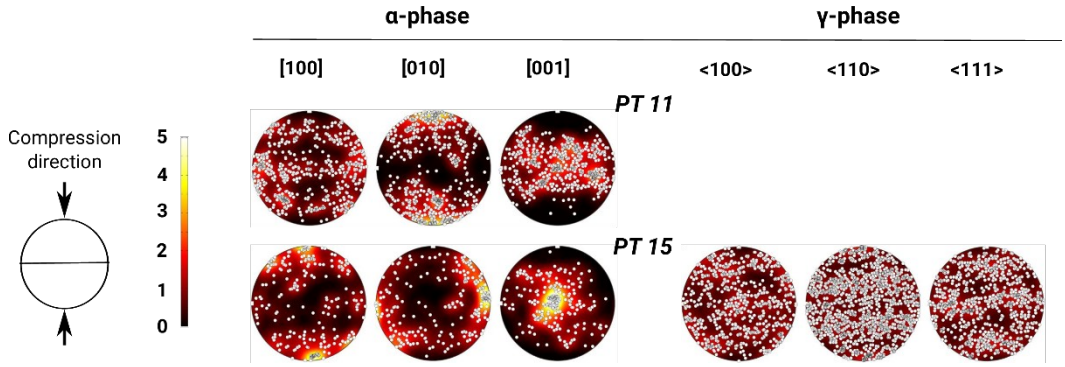

Figure 9: Sample results from multigrain crystallography in the DAC (Rosa et al. 2016). Pole figures presenting the orientations of individual olivine and ringwoodite grains during a phase transformation at ≈18 GPa and 880 K. White circles are individual grain orientations. Background color scale is recalculated based on an orientation distribution function fitted to sample. Scale in m.r.d. (multiples of a random distribution).

3.3.2 Defects

X-ray line profile analysis (XLPA) is an effective technique for the study of grain level microstructures using x-ray diffraction (Kerber et al. 2011). The shape of Bragg diffraction peaks can be quantitatively evaluated not only in terms of the crystallite size and its distribution, but also in terms of the density, type and arrangement of dislocations, twins and stacking faults (e.g. Fig. 10).

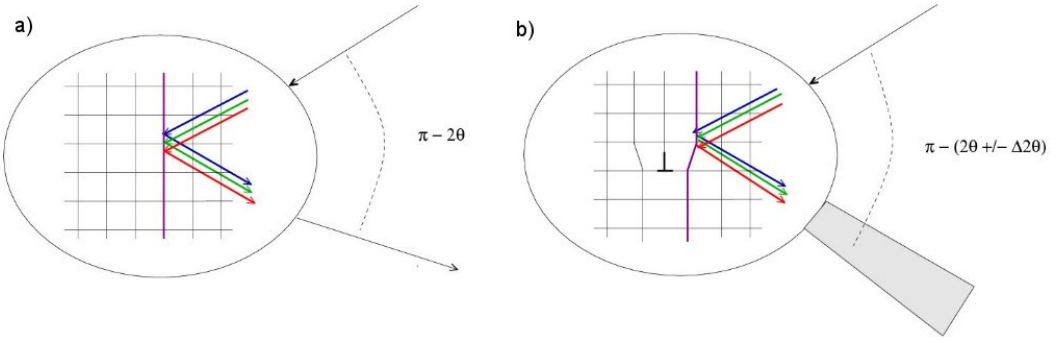

Figure 10: Principles of defect analysis using x-ray diffraction. Unlike a perfect crystal (a), defects such as dislocations induce a local distortion of the crystal structure (b). The presence of defects induces a broadening of the x-ray diffraction peak which, unlike that of grain sizes for instance, is anisotropic and depends on the hkl indices of the reflection and the type of dislocation.

The advantages of the XPLA method are that *i)* the resolution increases with a decreasing grain size and increasing defect density, and *ii)* it relies on x-ray diffraction and can hence be applied to high pressure experiments. The effect of dislocations on peak broadening, for instance, can be measured when their density increases above 10^{12} m^{-2}. On the other hand, it requires a high angular resolution (below 0.01°) and relative accuracy of 10^{-4} on diffraction intensities at the edges of diffraction peaks. Also note that, unlike techniques such as high resolution back-scattered electron diffraction (HR-EBSD), XLPA is

12

sensitive to the total dislocation density, including both geometrically necessary and statistically stored dislocations (Ribárik et al, 2019) and can not distinguish between both.

Under high pressure, the XPLA technique, combined with multigrain crystallography was used for the study of dislocations in deep Earth materials. Experiments on $MgGeO_3$ in the post-perovskite structure, for instance, allowed the identification of dominant dislocation types in this material at 90 GPa (Nisr et al. 2012).

4 Sample results

4.1 Deep Earth materials

Iron is one of the most abundant metals, a widely used technological material, and the main constituent of the Earth's core. As such, the plastic properties of iron under pressure and temperature have received much attention during the past decades. Nothing was known on the plasticity of ε-Fe in the mid-1990's and geophysical models of inner-core behavior often relied on simple assumptions such as the comparison of *c*/*a* ratios between ε-Fe and other hcp metals (e.g. Jeanloz and Wenk 1988). Pioneering works were performed at the Geophysical Laboratory with radial x-ray diffraction on Fe up to 220 GPa (Mao et al. 1998) and paved the way to the determination of the plastic properties of ε-Fe under high pressure (Wenk et al. 2000, Merkel et al. 2004, 2012, Gleason and Mao 2013, Nishihara et al. 2018).

Our current understanding is that basal slip and tensile twinning are the dominant plastic deformation mechanism of ε-Fe at high pressure and room temperature (Wenk et al. 2000, Merkel et al. 2012). The strength of each deformation was characterized with D-DIA measurements at 13–17 GPa and 400–700 K (Merkel et al. 2012, Nishihara et al. 2018). These new interpretations also highlight the important contribution of tensile twinning to understand the evolution of stress and texture at those conditions. Measurements up to 200 GPa at ambient temperature combined with a numerical model also indicate that the bulk shear strength of Fe is ≈1 GPa at inner-core pressures and temperatures (Gleason and Mao 2013). This suggests that the inner core is rheologically weak and supports dislocation creep as the dominant creep mechanism influencing deformation. Deformation experiments on Fe, however, have only reached pressures of ≈200 GPa at ambient temperature and combined pressure and temperatures of ≈17 GPa and ≈700 *K*. These remain far from those in the inner core (above 300 GPa and 5000 K). Future efforts will be hence invested in extending the pressure and temperature range of experiments analyzing the plastic behavior of Fe.

Ferropericlase, (Mg,Fe)O, is another interesting material regarding high pressure plasticity studies. MgO is a very well-known crystalline ceramic whose mechanical properties are thoroughly studied in materials science (Amodeo et al. 2018), both experimentally (e.g. Korte and Clegg 2011, Tromas et al. 2000) and using numerical plasticity techniques (e.g. Amodeo et al. 2012, Cordier et al. 2012). (Mg,Fe)O is also the second dominant phase in the Earth's lower mantle. For the above reasons, numerous studies of the plastic properties of (Mg,Fe)O under high pressure and temperature can be found in the literature (e.g.

Merkel et al. 2002, Cordier et al. 2012, Amodeo et al. 2012, 2016, Yamazaki and Karato 2002, Tommaseo et al. 2006, Lin et al. 2009, Long et al. 2006, Mei et al. 2008, Uchida et al. 2004, Lin et al. 2017, Marquardt and Miyagi 2015, Immoor et al. 2018, Kinsland and Bassett 1977, Lin et al. 2019, Girard et al. 2012, Heidelbach et al. 2003, Stretton et al. 2001).

Under ambient temperature, pure MgO deforms through dislocation slip on $\{110\}\langle 1\bar{1}0\rangle$ (Merkel et al. 2002, Lin et al. 2017) with an increased activity of $\{110\}\langle 100\rangle$ with increasing temperature (Paterson and Weaver 1970). Recent calculations also predict a transition between $\{110\}\langle 1\bar{1}0\rangle$ and $\{110\}\langle 100\rangle$ slip with increasing pressure (Amodeo et al. 2012) and that, moreover, in the Earth's mantle, extremely low strain rates counteract the influence of pressure with MgO deforming in the athermal regime where dislocation motion is purely controlled by dislocation interactions rather than lattice friction (Cordier et al. 2012). Deformation experiments on single crystal do show a trend consistent with such change of slip system with pressure (Girard et al. 2012) and deformation experiments on ferropericlase show evidence of both $\{110\}\langle 1\bar{1}0\rangle$ and $\{110\}\langle 100\rangle$ slip at ≈1400 K in a range of 30–60 GPa (Immoor et al. 2018). Recent ambient temperature measurements and modeling on pure MgO up to 50 GPa, however, predict an increasing activity of $\{110\}\langle 1\bar{1}0\rangle$ slip with pressure (Lin et al. 2019). As such, the effect of pressure (and strain rate) on the plasticity of pure MgO remains an active field of research.

The addition of Fe in (Mg,Fe)O does not seem to drastically affect the type of dominant slip systems in (Mg,Fe)O (Tommaseo et al. 2006, Long et al. 2006, Yamazaki and Karato 2002, Stretton et al. 2001, Immoor et al. 2018). Between 40 and 80 GPa however, Fe in (Mg,Fe)O undergoes electronic spin-pairing transition from a high-spin to a low-spin state (Badro et al. 2003) with potential effects of on sample stress (Lin et al. 2009). Measurements up to 100 GPa at ambient temperature also seem to indicate that the strength of (Mg,Fe)O increases by a factor of three at pressures from 20 to 65 GPa (Marquardt and Miyagi 2015) with important consequences regarding the stagnation of slabs sinking through the shallow lower mantle. These conclusions remain to be confirmed at mantle temperatures and strain rates.

4.2 Materials science

Simple metals were quickly recognized as a field of study regarding high pressure mechanical properties (e.g. Re, Mo and Au, Duffy et al. 1999b, 1999a). These first publications were followed by studies on Pt (Kavner and Duffy 2003), Os (Chen et al. 2010a, Weinberger et al. 2008), Gd (Xiong et al. 2014), W (He and Duffy 2006, Xiong et al. 2018), Co (Merkel et al. 2009), or Al (Singh et al. 2007), slowly constituting a database of strength and deformation mechanisms in simple metals as a function of pressure. It turns out that the yield strength of Os is significant larger than that of other stiff pure metals (≈12 GPa at 60 GPa), followed by Re and W. Other metals, such as Ti or Zr, undergo phase transitions at relatively low pressure. This motivated studies of texture and strength, both during the phase transformation and for the higher pressure phase. Wenk et al. (2013), for instance, studied the $\alpha \leftrightarrow \omega$ transition in Zr and found *i)* a martensitic mechanisms with $\langle 0001\rangle_\alpha \parallel \langle 11\bar{2}0\rangle_\beta$ and *ii)* remarkable orientation memory during the

14

reverse transformation. This was then followed by further studies on the $\alpha \leftrightarrow \omega$ transition in Zr and the mechanical properties of both phases (Yu et al. 2015, Kumar et al. 2020), with the aim to design Zr microstructure and strengthen its mechanical properties for high-pressure applications.

The Hall-Petch relationship predicts that the strength of materials should increase with smaller grain sizes. It is verified down to grain sizes of about 30 nm for which an inverse Hall-Petch effect is often observed, with a decrease of strength with decreasing grain size. This inverse Hall-Petch effect is attributed to a transition from dislocation-based plasticity to grain boundary sliding, rotation, or diffusion but this remains controvertial (Naik and Walley 2020). This motivated studies on the effect of grain sizes on the plastic behavior of nanocrystalline materials under pressure (e.g. Singh et al. 2008). The application of hydrostatic pressure is found to have a strong effect on the transition from the Hall-Petch to inverse Hall-Petch effect. In fact, evidences for dislocation activity were observed in 3 nm Ni compressed to 18.5 GPa (Chen et al. 2012). Moreover, recent work on pure Ni report a continuous strengthening in samples with grain sizes from 200 nm down to 3 nm, with the strengthening enhanced (rather than reduced) at grain sizes smaller than 20 nanometres (Zhou et al. 2020). These recent works await confirmation in other materials and a better understanding of the combined effect of pressure and grain sizes on dislocation-based plasticity. They do, however, illustrate how studies under high pressure can help solve fundamental issues in materials science.

Other applications in materials science include the design of new, strong materials either as pure phases (Xiong et al. 2013, Kiefer et al. 2005, Dong et al. 2009, He et al. 2004, Liermann et al. 2007, Chen et al. 2010b) or with a controlled microstructure (Conil and Kavner 2006), as well as the peculiar effect of phase transitions on microstructures in oxides (Yue et al. 2016). All remain an active field of study.

5 Perspectives

5.1 Multiphase aggregates

The vast majority of rocks that constitute the Earth are not made of a single material but rather an assemblage of multiple minerals. The microstructure, i.e. the arrangement of each phase, the orientation and size of each grain, has an influence on the overall mechanical properties of the rock. As such, the mechanical properties of multiphase aggregate are of great interest for the geosciences. They are also fundamental to materials science application, for which the design of composite materials with a pre-defined microstructure and physical properties are of great interest. Despite their relevance however, the mechanical properties of polyphase aggregates under pressure remain poorly understood.

In the Earth's lower mantle, for instance, bridgmanite is substantially stronger than ferropericlase and experiments indicate that ferropericlase accommodates most of the strain (Wang et al. 2013, Miyagi and Wenk 2016, Girard et al. 2016). A simple approach indicates that, if the weaker ferropericlase is not interconnected, then rheology of the lower mantle will mostly depend on bridgmanite, but if ferropericlase is interconnected, then it will control deformation. The microstructural arrangement of

bridgmanite and ferropericlase, however, is controlled by plastic deformation, which in turn, is controlled by the properties of both phases. It is therefore required to understand this complex interplay between microstructure, the properties of each phase, and the material's macroscopic response. Moreover, stress percolates through polycrystalline materials that have heterogeneous elastic and plastic properties. The pattern of stress percolation is related to the degree of heterogeneity in and statistical distribution of the elastic and plastic properties of the constituent grains in the aggregate (Burnley 2013). To this day, the understanding and modeling of the feedback between single phase plasticity, microstructures, and macroscopic behavior of multiphase materials remains a challenge that has seldomly been attempted in high pressure research (Kaercher et al. 2016, Kasemer et al. 2020).

In addition, pressure, temperature, and deformation can induce mineralogical reactions which will affect the mechanical properties of the aggregate. In olivine + serpentines aggregates, for instance, it has been shown that dehydration reactions of deforming samples containing only 5 vol% of antigorite suffices to trigger significant stress transfer and embrittlement (Ferrand et al. 2017). A strong weakening of cold subducting slab was also reported due to the olivine to ringwoodite phase transformation (Mohiuddin et al. 2020). The mechanical properties of aggregates undergoing phase transformations are relevant for mantle dynamics and the generation of deep earthquakes deep inside the Earth. Such approach could, also, find multiple application for the understanding of mechanical properties of materials undergoing phase transformations at other conditions of extreme pressure and temperature.

5.2 Technical developments

This chapter mostly focused on coupling in-situ deformation, x-ray diffraction, and radiography. In the coming years, high pressure deformation studies could greatly benefit from further technological developments. For the study of deep earthquakes for instance, the D-DIA deformation press has been coupled with devices recording the sample's acoustic emissions during deformation (Schubnel et al. 2013). The acoustic emission signals can even be further processed to understand the nature of the focal mechanisms, their distribution in both space and time during deformation, and further waveform analysis could be possible (Wang et al. 2017). The combination of high pressure plastic deformation experiments with the tracking of the sample's acoustic emissions could be of great interest for high pressure plasticity studies. In fact, plastic mechanisms such as twinning or dislocation slip are known to trigger acoustic emissions in ambient pressure deformation experiments (Weiss et al. 2000, Vinogradov et al. 2016, Muránsky et al. 2010) and this field of study could open new doors to high pressure research.

Presently, strain measurements in DAC deformation experiments is limited to average measurements in polycrystals. Multigrain crystallography allows strain mapping at the grain level (Oddershede et al. 2010) and can be used, for instance, to evaluate strain localization in deformation experiments (Sedmák et al. 2016). Strain mapping using multigrain crystallography has been tested in DAC experiments (Nisr et al. 2014) but the method remains to be strengthened, tested, and applied to topics such as stress percolation in heterogeneous aggregates.

Advanced imaging techniques, often relying on the high coherence of synchrotron x-ray beams, such as Bragg coherent diffractive imaging, ptychography, or dark-field x-ray microscopy, allow for revealing strains and heterogeneities within a single grain (Yau et al. 2017, Hruszkewycz et al. 2016, Simons et al. 2015), may be used under operando conditions, and some have been tested in DAC experiments (Yang et al. 2013). These proof-of-concept experiments show that three-dimensional strain distribution with a spatial resolution of 30 nm can be measured inside a 400 nm crystal within a DAC. At present, these techniques represent a steep technical challenge but, with the advent of new, powerful, and highly coherent sources at ERSF, PETRA, SPRING-8, and APS, may become more routine measurements in the future. Local strain mapping techniques allowing, for instance, the determination and mapping of dislocation types and densities (Wallis et al. 2017) could then be performed in situ under high pressure.

3D X-ray tomography also offers avenues for new experiments in LVP (e.g. Urakawa et al. 2010, Wang et al. 2011, Philippe et al. 2016, Yu et al. 2016) with the ability to resolve small heterogeneities under high pressure and temperature and various strain conditions. This allows in situ tracking of various components in complex materials, with implications on their mechanical properties, connectivity, or permeability. Wang et al (2011) and Todd et al (2016), for instance, studied the effect of deformation on microstructures of metal-silicate aggregates with implications for the mechanical properties of composite materials relevant to the Earth's mantle and the formation of planetary cores. One could also refer to ongoing on work on serpentines-olivine aggregates, with implications for subduction zones (Mandolini et al. 2020) or the in-situ monitoring of the orientations and mobility of interfaces during phase transitions (e.g. Boulard et al. 2020).

Finally, the present chapter focused on measurements performed in "static" experiments. With the advent of gas-gun or laser-driven dynamic compression techniques coupled with either synchrotron or x-ray free electron lasers and faster detectors, time-resolved measurements at rapid strain rates are now achievable (e.g. Wehrenberg et al, 2017, Chen et al, 2019). Combined with deformation experiments at low strain rates, as described in this chapter, intermediate strain rate experiments in a dynamic diamond anvil cell (Méndez et al, 2020), and dynamic compression experiments will allow investigating the effect of orders of magnitude in strain rate on deformation and plasticity.

6 Conclusion

This chapter summarized the last 25 years of development of high pressure measurements of mechanical properties. The team around H.-K. Mao at the Carnegie Institution pioneered the development of radial x-ray diffraction in the DAC. The following years saw the development of LVP experiments, external-heating radial x-ray diffraction in the DAC, or multigrain crystallography. Conceptual advances, from the first theories of lattice strains in the 1990's to more advanced self-consistent calculations have also been a key component of such research. Early results and interpretation of high pressure deformation experiments lacked understanding of the fundamentals of plasticity and its effect on materials properties

and x-ray diffraction measurements. The introduction of self-consistent calculations was hence an important contribution to the field.

Nowadays, the studies of mechanical properties under extreme conditions is a thriving field of research, with applications in geosciences, for which it was first intended, but also materials sciences, as highlighted in the latest section of this chapter. Recent works, relying on multi-grain crystallography now allow the study of microstructures and plasticity at the grain scale and will open new doors to this field of research, offering a quantitative and comprehensive description of materials microstructure at the micrometre lengthscale. Strain mapping within a grain, along with the identification of deformation defects and densities is also within reach.

Plasticity depends on pressure, temperature, microstructures, but also strain rates. Further works should hence not only focus on extending the pressure and temperature conditions of the experiments, in order to reach those of the innermost sections of our planet, but also on exploring strain rates, from extremely fast processes at 10^{10} s^{-1} in a shock wave, to deep Earth conditions of 10^{-15} s^{-1}. To this day, this remains an experimental and numerical challenge.

Acknowledgments

The author would like to thank the two anonymous reviewers and N. Hilairet for constructive comments, as well as F. Lin for providing the raw data for Fig. 7. S. M. received support from the I-SITE UNLE grant MetalCore (R-ERCGEN-19-006-MERKEL).

18

References

Amodeo, J., Carrez, P. & Cordier, P. (2012). Modelling the effect of pressure on the critical shear stress of MgO single crystals. Phil. Mag., 92, 1523–1541.

Amodeo, J., Dancette, S. & Delannay, L. (2016). Atomistically-informed crystal plasticity in MgO polycrystals under pressure. Int. J. Plast., 82, 177–191.

Amodeo, J., Merkel, S., Tromas, C., Carrez, P., Korte-Kerzel, S., Cordier, P. & Chevalier, J. (2018). Dislocations and plastic deformation in MgO crystals: A review. Crystals, 8, 240.

Azuma, S., Nomura, R., Uesugi, K., Nakashima, Y., Kojima, Y., Doi, S. & Kakizawa, S. (2017). Anvil design for slip-free high pressure deformation experiments in a rotational diamond anvil cell. High Pressure Research, 38(1), 23–31.

Badro, J., Fiquet, G., Guyot, F., Rueff, J.-P., Struzhkin, V. V., Vankó, G. & Monaco, G. (2003). Iron partitioning in earth's mantle: Toward a deep lower mantle discontinuity. Science, 300, 789–791.

Blank, V., Konyaev, Y. S., Kuznetsov, A. I. & Estrin, E. (1984). Diamond chamber for examining the effects of shear deformation on the structure and properties of solids at pressures up to 43 GPa. *Instrum.* Exp. Tech., 27, 1240–1242.

Boioli, F., Carrez, P., Cordier, P., Devincre, B., Gouriet, K., Hirel, P., Kraych, A. & Ritterbex, S. (2017). Pure climb creep mechanism drives flow in Earth's lower mantle. Sci. Adv., 3(3), e1601958.

Boulard, E., Denoual, C., Dewaele, A., King, A., Godec, Y. L. & Guignot, N. (2020) Following the phase transitions of iron in 3D with X-ray tomography and diffraction under extreme conditions. Acta Mater., 192, 30-39

Burnley, P. (2013). The importance of stress percolation patterns in rocks and other polycrystalline materials. Nature Communications, 4(1), 2117.

Chen, S., Li, Y., Zhang, N., Huang, J., Hou, H., Ye, S., Zhong, T., Zeng, X., Fan, D., Lu, L., Wang, L., Sun, T., Fezzaa, K., Zhang, Y., Tang, M. & Luo, S. (2019). Capture Deformation Twinning in Mg during Shock Compression with Ultrafast Synchrotron X-Ray Diffraction. Phys. Rev. Lett., 123, 255501

Chen, B., Lutker, K., Raju, S. V., Yan, J., Kanitpanyacharoen, W., Lei, J., Yang, S., Wenk, H.-R., Mao, H.-K. & Williams, Q. (2012). Texture of nanocrystalline nickel: Probing the lower size limit of dislocation activity. Science, 338(6113), 1448–1451.

Chen, H., He, D., Liu, J., Li, Y., Peng, F., Li, Z., Wang, J. & Bai, L. (2010a). High-pressure radial x-ray diffraction study of osmium to 58 GPa. Eur. Phys. J. B, 73, 321–326.

Chen, H., Peng, F., Mao, H.-K., Shen, G., Liermann, H.-P., Li, Z. & Shu, J. (2010b). Strength and elastic moduli of TiN from radial x-ray diffraction under nonhydrostatic compression up to 45 GPa. J. Appl. Phys., 107(11), 113503.

Clausen, B., Tomé, C. N., Brown, D. W. & Agnew, S. R. (2008). Reorientation and stress relaxation due to twinning: Modeling and experimental characterization for Mg. Acta Mater., 56, 2456–2468.

566 Conil, N. & Kavner, A. (2006). Elastic behavior and strength of Al_2O_3 fiber/Al matrix composite and
567 implications for equation of state measurements in the diamond anvil cell. J. Appl. Phys., 100,
568 043517.
569 Cordier, P., Amodeo, J. & Carrez, P. (2012). Modelling the rheology of MgO under Earth's mantle
570 pressure, temperature and strain rates. Nature, 481, 177-180.
571 Cordier, P. & Goryaeva, A. (Eds.) (2018). Multiscale Modeling of the Mantle Rheology. Lille, France.
572 https://lilloa.univ-lille.fr/handle/20.500.12210/5756
573 Dewaele, A., Loubeyre, P., Occelli, F., Marie, O. & Mezouar, M. (2018). Toroidal diamond anvil cell for
574 detailed measurements under extreme static pressures. Nat. Commun., 9(1).
575 Dobson, D. P., Miyajima, N., Nestola, F., Alvaro, M., Casati, N., Liebske, C., Wood, I. G. & Walker,
576 A. M. (2013). Strong inheritance of texture between perovskite and post-perovskite in the D"
577 layer. Nat. Geosci., 6, 575-578.
578 Dong, H., He, D., Duffy, T. S. & Zhao, Y. (2009). Elastic moduli and strength of nanocrystalline cubic
579 BC_2N from x-ray diffraction under nonhydrostatic compression. Phys. Rev. B, 79, 014105.
580 Duffy, T. S., Shen, G., Heinz, D. L., Shu, J., Ma, Y., Mao, H. K., Hemley, R. J. & Singh, A. K. (1999a).
581 Lattice strains in gold and rhenium under non-hydrostatic compression to 37 GPa. Phys. Rev. B,
582 60, 15063–15073.
583 Duffy, T. S., Shen, G., Shu, J., Mao, H. K., Hemley, R. J. & Singh, A. K. (1999b). Elasticity, shear
584 strength and equation of state of molybdenum and gold from x-ray diffraction under
585 nonhydrostatic compression to 24 GPa. J. Appl. Phys., 86, 6729–6736.
586 Farla, R., Amulele, G., Girard, J., Miyajima, N. & Karato, S.-I. (2015). High-pressure and high-
587 temperature deformation experiments on polycrystalline wadsleyite using the rotational drickamer
588 apparatus. Phys. Chem. Min., 42, 541–558.
589 Ferrand, T. P., Hilairet, N., Incel, S., Deldicque, D., Labrousse, L., Gasc, J., Renner, J., Wang, Y., II, H.
590 W. G. & Schubnel, A. (2017). Dehydration-driven stress transfer triggers intermediate-depth
591 earthquakes. Nat. Commun., 8, 15247.
592 Girard, J., Amulele, G., Farla, R., Mohiuddin, A. & Karato, S.-I. (2016). Shear deformation of
593 bridgmanite and magnesiowüstite aggregates at lower mantle conditions. Science, 351, 144–147.
594 Girard, J., Chen, J. & Raterron, P. (2012). Deformation of periclase single crystals at high pressure and
595 temperature: Quantification of the effect of pressure on slip-system activities. J. Appl. Phys., 111,
596 112607.
597 Girard, J., Silber, R. E., Mohiuddin, A., Chen, H. & Karato, S. (2020) Development of a Stress Sensor for
598 In-Situ High-Pressure Deformation Experiments Using Radial X-Ray Diffraction. Minerals, 10,
599 166
600 Gleason, A. E. & Mao, W. L. (2013). Strength of iron at core pressures and evidence for a weak Earth's
601 inner core. Nat. Geosci., 6, 571-574.
602 He, D. & Duffy, T. S. (2006). X-ray diffraction study of the static strength of tungsten to 69 GPa. Phys.
603 Rev. B, 73(13).

He, D., Shieh, S. & Duffy, T. (2004). Strength and equation of state of boron suboxide from radial x-ray diffraction in a diamond cell under nonhydrostatic compression. Phys. Rev. B, 70, 184121.

Heidelbach, F., Stretton, I., Langenhorst, F. & Mackwell, S. (2003). Fabric evolution during high shear strain deformation of magnesiowüstite ($Mg_{0.8}Fe_{0.2}$ O). J. Geophys. Res., 108, 2154.

Hemley, R. J., Mao, H. K., Shen, G., Badro, J., Gillet, P., Hanfland, M. & Häusermann, D. (1997). X-ray imaging of stress and strain of diamond, iron & tungsten at megabar pressures. Science, 276, 1242–1245.

Hruszkewycz, S. O., Allain, M., Holt, M. V., Murray, C. E., Holt, J. R., Fuoss, P. H. & Chamard, V. (2016). High-resolution three-dimensional structural microscopy by single-angle bragg ptychography. Nature Materials, 16(2), 244–251.

Hunt, S. A. & Dobson, D. P. (2017). Note: Modified anvil design for improved reliability in DT-cup experiments. Rev. Sci. Instrum., 88, 126106.

Hunt, S. A., Weidner, D. J., McCormack, R. J., Whitaker, M. L., Bailey, E., Li, L., Vaughan, M. T. & Dobson, D. P. (2014). Deformation T-Cup: A new multi-anvil apparatus for controlled strain-rate deformation experiments at pressures above 18 GPa. Rev. Sci. Instrum., 85, 085103.

Ice, G. E., Dera, P., Liu, W. & Mao, H.-K. (2005). Adapting polychromatic x-ray microdiffraction techniques to high-pressure research: energy scan approach. J. Synchrotron Rad., 12, 608–617.

Immoor, J., Marquardt, H., Miyagi, L., Lin, F., Speziale, S., Merkel, S., Buchen, J., Kurnosov, A. & Liermann, H.-P. (2018). Evidence for {100}<011> slip in ferropericlase in earth's lower mantle from high-pressure/high-temperature experiments. Earth Planet. Sci. Lett., 489, 251–257.

Immoor, J., Marquardt, H., Miyagi, L., Speziale, S., Merkel, S., Schwark, I., Ehnes, A. & Liermann, H.-P. (2020). An improved setup for radial diffraction experiments at high pressures and high temperatures in a resistive graphite-heated diamond anvil cell. Rev. Sci. Instrum., 91(4), 045121.

Jeanloz, R. & Wenk, H.-R. (1988). Convection and anisotropy of the inner core. Geophys. Res. Lett., 15, 72–75.

Kaercher, P., Miyagi, L., Kanitpanyacharoen, W., Zepeda-Alarcon, E., Wang, Y., Parkinson, D., Lebensohn, R., Carlo, F. D. & Wenk, H. (2016). Two-phase deformation of lower mantle mineral analogs. Earth Planet. Sci. Lett., 456, 134–145.

Karato, S.-I., Forte, A., Liebermann, R., Masters, G. & Stixrude, L. (Eds.) (2000). Earth's Deep Interior: Mineral Physics and Tomography From the Atomic to the Global Scale. Geophysical Monograph Series. Washington, DC: American Geophysical Union.

Kasemer, M., Zepeda-Alarcon, E., Carson, R., Dawson, P. & Wenk, H.-R. (2020). Deformation heterogeneity and intragrain lattice misorientation in high strength contrast, dual-phase bridgmanite/periclase. Acta Mater., 189, 284–298.

Kavner, A. & Duffy, T. S. (2003). Elasticity and rheology of platinum under high pressure and nonhydrostatic stress. Phys. Rev. B, 68, 144101.

Kawazoe, T., Karato, S. &o, J., Jing, Z., Otsuka, K. & Hustoft, J. W. (2010). Shear deformation of polycrystalline wadsleyite up to 2100 K at 14-17 GPa using a rotational drickamer apparatus (RDA). J. Geophys. Res., 115, B08208.

Kawazoe, T., Ohuchi, T., Nishihara, Y., Nishiyama, N., Fujino, K. & Irifune, T. (2013). Seismic anisotropy in the mantle transition zone induced by shear deformation of wadsleyite. Phys. Earth Planet. Int., 216, 91–98.

Kerber, M. B., Zehetbauer, M. J., Schafler, E., Spieckermann, F. C., Bernstorff, S. & Ungar, T. (2011). X-ray line profile analysis – An ideal tool to quantify structural parameters of nanomaterials. JOM, 63, 61–70.

Kiefer, B., Shieh, S. R., Duffy, T. S. & Sekine, T. (2005). Strength, elasticity, and equation of state of the nanocrystalline cubic silicon nitride γ-Si_3N_4 to 68 GPa. Phys. Rev. B, 72, 014102.

Kinsland, G. L. & Bassett, W. A. (1977). Strength of MgO and NaCl polycrystals to confining pressures of 250 kbar at 25 C. J. Appl. Phys., 48, 978–984.

Kocks, U. F., Tomé, C. N. & Wenk, H.-R. (1998). Texture and Anisotropy: Preferred Orientations and their Effects on Material Properties. Cambridge: Cambridge Univ. Press.

Korte, S. & Clegg, W. (2011). Discussion of the dependence of the effect of size on the yield stress in hard materials studied by microcompression of MgO. Philos. Mag., 91(7-9), 1150–1162.

Kumar, M. A., Hilairet, N., McCabe, R., Yu, T., Wang, Y., Beyerlein, I. & Tomé, C. (2020). Role of twinning on the omega-phase transformation and stability in zirconium. Acta Mater., 185, 211–217.

Langrand, C., Hilairet, N., Nisr, C., Roskosz, M., Ribárik, G., Vaughan, G. B. M. & Merkel, S. (2017). Reliability of multigrain indexing for orthorhombic polycrystals above 1mbar: application to $MgSiO_3$ post-perovskite. J. Appl. Crystallogr., 50, 120–130.

Lebensohn, R. A. & Tomé, C. N. (1994). A self-consistent visco-plastic model: calculation of rolling textures of anisotropic materials. Mater. Sci. Eng. A, 175, 71–82.

Levitas, V. I. (2004). High-pressure mechanochemistry: Conceptual multiscale theory and interpretation of experiments. Phys. Rev. B, 70, 184118.

Li, L., Weidner, D. J., Chen, J., Vaughan, M. T., Davis, M. & Durham, W. B. (2004). X-ray strain analysis at high pressure: Effect of plastic deformation in MgO. J. Appl. Phys., 95, 8357–8365.

Liermann, H.-P., Merkel, S., Miyagi, L., Wenk, H.-R., Shen, G., Cynn, H. & Evans, W. J. (2009). New experimental method for in situ determination of material textures at simultaneous high-pressure and temperature by means of radial diffraction in the diamond anvil cell. Rev. Sci. Instrum., 80, 104501.

Liermann, H. P., Singh, A. K., Somayazulu, M. & Saxena, S. K. (2007). Compression behavior of NbC under nonhydrostatic conditions to 57 GPa. Int. J. Refract. Met. Hard Mater., 25, 386–391.

Lin, F., Couper, S., Jugle, M. & Miyagi, L. (2019). Competing deformation mechanisms in periclase: Implications for lower mantle anisotropy. Minerals, 9, 650.

Lin, F., Hilairet, N., Raterron, P., Addad, A., Immoor, J., Marquardt, H., Tomé, C., Miyagi, L. & Merkel, S. (2017). Elasto-viscoplastic self consistent modeling of the ambient temperature plastic behavior of periclase deformed up to 5.4 GPa. J. Appl. Phys., 122, 205902.

Lin, J. F., Wenk, H.-R., Voltolini, M., Speziale, S., Shu, J. & Duffy, T. S. (2009). Deformation of lower-mantle ferropericlase (Mg,Fe)O across the electronic spin transition. Phys. Chem. Min., 36, 585–592.

Lincot, A., Cardin, P., Deguen, R. & Merkel, S. (2016). Multiscale model of global inner-core anisotropy induced by hcp alloy plasticity. Geophys. Res. Lett., 43, 1084–1091.

Long, M. D., Xiao, X., Jiang, Z., Evansa, B. & Karato, S. (2006). Lattice preferred orientation in deformed polycrystalline (Mg,Fe)O and implications for seismic anisotropy in D". Phys. Earth Planet. Inter., 156, 75–88.

Ludwig, W., King, A., Reischig, P., Herbig, M., Lauridsen, E., Schmidt, S., Proudhon, H., Forest, S., Cloetens, P., du Roscoat, S. R., Buffière, J., Marrow, T. & Poulsen, H. (2009). New opportunities for 3D materials science of polycrystalline materials at the micrometre lengthscale by combined use of x-ray diffraction and x-ray imaging. Mat. Sci. Eng. A, 524, 69–76.

Lutterotti, L., Matthies, S. & Wenk, H.-R. (1999). MAUD: a friendly Java program for materials analysis using diffraction. IUCr: Newsletter of the CPD, 21, 14–15.

Ma, Y., Selvi, E., Levitas, V. I. & Hashemi, J. (2006). Effect of shear strain on the α−ε phase transition of iron: a new approach in the rotational diamond anvil cell. J. Phys.: Condens. Matter, 18, S1075–S1082.

Mainprice, D., Barruol, G. & Ismaïl, W. B. (2000). The seismic anisotropy of the earth's mantle: from single crystal to polycrystal. In S. Karato, A. M. Forte, R. C. Liebermann, G. Master & L. Stixrude (Eds.) Earth's Deep Interior. Mineral Physics and Tomography. From the Atomic to the Global Scale, (pp. 237–264). Washington, DC: Am. Geophys. Union.

Mandolini, T., Hilairet, N., Chantel, J., Merkel, S., Le Godec, Y., Guignot, N. & King, A. (2020) Microstructural evolution in deforming olivine-serpentine aggregates at subduction zones conditions using in-situ X-ray tomography, AGU Fall Meeting, MR028-06

Mao, H. K., Shu, J., Shen, G., Hemley, R. J., Li, B. & Singh, A. K. (1998). Elasticity and rheology of iron above 220 GPa and the nature of the earth's inner core. Nature, 396, 741–743. Correction, Nature 399, 280, 1999.

Marquardt, H. & Miyagi, L. (2015). Slab stagnation in the shallow lower mantle linked to an increase in mantle viscosity. Nat. Geosci., 8, 311–314.

Meade, C. & Jeanloz, R. (1988) Yield strength of MgO to 40 GPa. J. Geophys. Res., 93, 3261–3269

Mei, S., Kohlstedt, D. L., Durham, W. B. & Wang, L. (2008). Experimental investigation of the creep behavior of MgO at high pressures. Phys. Earth Planet. Inter., 170, 170–175.

Méndez, A. S. J., Marquardt, H., Husband, R. J., Schwark, I., Mainberger, J., Glazyrin, K., Kurnosov, A., Otzen, C., Satta, N., Bednarcik, J. & Liermann, H.-P. (2020) A resistively-heated dynamic diamond anvil cell (RHdDAC) for fast compression x-ray diffraction experiments at high temperatures. Rev. Sci. Instrum., 91, 073906

Merkel, S., Gruson, M., Wang, Y., Nishiyama, N. & Tomé, C. N. (2012). Texture and elastic strains in hcp-iron plastically deformed up to 17.5 GPa and 600 K: experiment and model. Modelling Simul. Mater. Sci. Eng., 20, 024005.

719 Merkel, S. & Hilairet, N. (2015). Multifit/polydefix: a framework for the analysis of polycrystal
720 deformation using x-rays. J. Appl. Cryst., 48, 1307–1313.
721 Merkel, S., McNamara, A. K., Kubo, A., Speziale, S., Miyagi, L., Meng, Y., Duffy, T. S. & Wenk, H.-R.
722 (2007). Deformation of (Mg,Fe)SiO_3 post-perovskite and D" anisotropy. Science, 316, 1729 –
723 1732.
724 Merkel, S., Miyajima, N., Antonangeli, D., Fiquet, G. & Yagi, T. (2006). Lattice preferred orientation and
725 stress in polycrystalline hcp-Co plastically deformed under high pressure. J. Appl. Phys., 100,
726 023510.
727 Merkel, S., Tomé, C. N. & Wenk, H.-R. (2009). A modeling analysis of the influence of plasticity on high
728 pressure deformation of hcp-Co. Phys. Rev. B, 79, 064110.
729 Merkel, S., Wenk, H.-R., Gillet, P., Mao, H. K. & Hemley, R. J. (2004). Deformation of polycrystalline
730 iron up to 30 GPa and 1000 K. Phys. Earth Planet. Inter., 145, 239–251.
731 Merkel, S., Wenk, H.-R., Shu, J., Shen, G., Gillet, P., Mao, H. K. & Hemley, R. J. (2002). Deformation of
732 polycrystalline MgO at pressures of the lower mantle. J. Geophys. Res., 107, 2271.
733 Merkel, S. & Yagi, T. (2005). X-ray transparent gasket for diamond anvil cell high pressure experiments.
734 Rev. Sci. Instrum., 76, 046109.
735 Miyagi, L., Amulele, G., Otsuka, K., Du, Z., Farla, R. & Karato, S. (2014). Plastic anisotropy and slip
736 systems in ringwoodite deformed to high shear strain in the rotational Drickamer apparatus. Phys.
737 Earth Planet. Int., 228, 244–253.
738 Miyagi, L., Kanitpanyacharoen, W., Kaercher, P., Lee, K. K. M. & Wenk, H.-R. (2010). Slip systems in
739 $MgSiO_3$ post-perovskite: Implications for D" anisotropy. Science, 329, 1639 – 1641.
740 Miyagi, L., Kunz, M., Knight, J., Nasiatka, J., Voltolini, M. & Wenk, H.-R. (2008). In situ phase
741 transformation and deformation of iron at high pressure and temperature. J. Appl. Phys., 104,
742 103510.
743 Miyagi, L., Kanitpanyacharoen, W., Raju, S. V., Kaercher, P., Knight, J., MacDowell, A., Wenk, H.-R.,
744 Williams, Q. & Alarcon, E. Z. (2013). Combined resistive and laser heating technique for in situ
745 radial X-ray diffraction in the diamond anvil cell at high pressure and temperature. Rev. Sci.
746 Instrum., 84, 025118
747 Miyagi, L. & Wenk, H.-R. (2016). Texture development and slip systems in bridgmanite and bridgmanite
748 + ferropericlase aggregates. Phys Chem Minerals, 43(8), 597–613.
749 Mohiuddin, A., Karato, S. & Girard, J. (2020) Slab weakening during the olivine to ringwoodite transition
750 in the mantle. Nat. Geosci., 13, 170-174
751 Muránsky, O., Barnett, M., Carr, D., Vogel, S. & Oliver, E. (2010). Investigation of deformation twinning
752 in a fine-grained and coarse-grained ZM20 mg alloy: Combined in situ neutron diffraction and
753 acoustic emission. Acta Mater, 58(5), 1503–1517.
754 Naik, S. N. & Walley, S. M. (2020). The hall–petch and inverse hall–petch relations and the hardness of
755 nanocrystalline metals. J. Mater. Sci., 55(7), 2661–2681.

Neil, C. J., Wollmershauser, J. A., Clausen, B., Tomé, C. N. & Agnew, S. R. (2010) Modeling lattice strain evolution at finite strains and experimental verification for copper and stainless steel using in situ neutron diffraction. Int. J. Plasticity, 26, 1772–1791

Nishihara, Y., Ohuchi, T., Kawazoe, T., Seto, Y., Maruyama, G., Higo, Y., Funakoshi, K.-I., Tange, Y. & Irifune, T. (2018). Deformation-induced crystallographic-preferred orientation of hcp-iron: An experimental study using a deformation-DIA apparatus. Earth Planet. Sci. Lett., 490, 151–160.

Nishihara, Y., Tinker, D., Kawazoe, T., Xu, Y., Jing, Z., Matsukage, K. N. & Karato, S. (2008). Plastic deformation of wadsleyite and olivine at high-pressure and high-temperature using a rotational Drickamer apparatus (RDA). Phys. Earth Planet. Inter., 170, 156–169.

Nisr, C., Ribárik, G., Ungár, T., Vaughan, G. B. & Merkel, S. (2014). Three-dimensional x-ray diffraction in the diamond anvil cell: application to stishovite. High Pres. Res., 34, 158–166.

Nisr, C., Ribárik, G., Ungár, T., Vaughan, G. B. M., Cordier, P. & Merkel, S. (2012). High resolution three-dimensional x-ray diffraction study of dislocations in grains of $MgGeO_3$ post-perovskite at 90 GPa. J. Geophys. Res., 117, B03201.

Nomura, R., Azuma, S., Uesugi, K., Nakashima, Y., Irifune, T., Shinmei, T., Kakizawa, S., Kojima, Y. & Kadobayashi, H. (2017). High-pressure rotational deformation apparatus to 135 GPa. Rev. Sci. Instrum., 88, 044501.

Noyan, I. & Cohen, J. (1987). Residual stress: measurements by diffraction and interpretation. New-York: Springer-Verlag.

Nzogang, B. C., Bouquerel, J., Cordier, P., Mussi, A., Girard, J. & Karato, S. (2018). Characterization by scanning precession electron diffraction of an aggregate of bridgmanite and ferropericlase deformed at HP-HT. Geochem. Geophys. Geosyst., 19(3), 582–594.

Oddershede, J., Schmidt, S., Poulsen, H. F., Sorensen, H. O., Wright, J. & Reimers, W. (2010). Determining grain resolved stresses in polycrystalline materials using three-dimensional x-ray diffraction. J. Appl. Cryst., 43, 539–549.

Paterson, M. S. & Weaver, C. W. (1970). Deformation of polycrystalline MgO under pressure. J. Am. Ceram. Soc., 53, 463–471.

Philippe, J., Godec, Y. L., Mezouar, M., Berg, M., Bromiley, G., Bergame, F., Perrillat, J. P., Alvarez-Murga, M., Morand, M., Atwood, R., King, A. & Régnier, S. (2016) Rotating tomography Paris–Edinburgh cell: a novel portable press for micro-tomographic 4-D imaging at extreme pressure/temperature/stress conditions. High Pressure Research, 36, 512-532

Poulsen, H. F. (2004). Three-Dimensional X-Ray Diffraction Microscopy: Mapping Polycrystals and their Dynamics. vol. 205 of Springer Tracts in Modern Physics. Berlin, Heidelberg, Germany: Springer.

Raterron, P. & Merkel, S. (2009). In situ rheological measurements at extreme pressure and temperature using synchrotron x-ray diffraction and radiography. J. Synchrotron Radiat., 16, 748–756.

Reali, R., Jackson, J., Orman, J. V., Bower, D., Carrez, P. & Cordier, P. (2019). Modeling viscosity of (Mg,Fe)O at lowermost mantle conditions. Phys. Earth Planet. Inter., 287, 65–75.

Reynard, B., Caracas, R., Cardon, H., Montagnac, G. & Merkel, S. (2019). High-pressure yield strength of rocksalt structures using quartz raman piezometry. C.R. Geosci., 351(2-3), 71–79.

Ribárik, G., Jóni, B. & Ungár, T. (2019) Global optimum of microstructure parameters in the CMWP line-profile-analysis method by combining Marquardt-Levenberg and Monte-Carlo procedures. J. Mater. Sci. Technol., 35, 1508-1514

Rosa, A. D., Hilairet, N., Ghosh, S., Perrillat, J.-P., Garbarino, G. & Merkel, S. (2016). Evolution of grain sizes and orientations during phase transitions in hydrous Mg_2SiO_4. J. Geophys. Res., 121, 7161–7176.

Schmidt, S. (2014). Grainspotter: a fast and robust polycrystalline indexing algorithm. J Appl Cryst, 47, 276–284.

Schropp, A., Hoppe, R., Meier, V., Patommel, J., Seiboth, F., Ping, Y., Hicks, D. G., Beckwith, M. A., Collins, G. W., Higginbotham, A., Wark, J. S., Lee, H. J., Nagler, B., Galtier, E. C., Arnold, B., Zastrau, U., Hastings, J. B. & Schroer, C. G. (2015). Imaging Shock Waves in Diamond with Both High Temporal and Spatial Resolution at an XFEL Sci. Rep., 5, 11089

Schubnel, A., Brunet, F., Hilairet, N., Gasc, J., Wang, Y. & Green II, H. W. (2013). Deep-focus earthquake analogs recorded at high pressure and temperature in the laboratory. Science, 341, 1377–1380.

Sedmák, P., Pilch, J., Heller, L., Kopeček, J., Wright, J., Sedlák, P., Frost, M. & Šittner, P. (2016). Grain-resolved analysis of localized deformation in nickel-titanium wire under tensile load. 353, 559–562.

Simons, H., King, A., Ludwig, W., Detlefs, C., Pantleon, W., Schmidt, S., Stöhr, F., Snigireva, I., Snigirev, A. & Poulsen, H. F. (2015). Dark-field x-ray microscopy for multiscale structural characterization. Nature Communications, 6(1), 6098.

Singh, A. K., Balasingh, C., Mao, H. K., Hemley, R. J. & Shu, J. (1998). Analysis of lattice strains measured under non-hydrostatic pressure. J. Appl. Phys., 83, 7567–7575.

Singh, A. K., Liermann, H., Akahama, Y., Saxena, S. K. & Menéndez-Proupin, E. (2008). Strength of polycrystalline coarse-grained platinum to 330 GPa and of nanocrystalline platinum to 70 GPa from high-pressure x-ray diffraction data. J. Appl. Phys., 103, 063524.

Singh, A. K., Liermann, H.-P., Akahama, Y. & Kawamura, H. (2007). Aluminum as a pressure-transmitting medium cum pressure standard for x-ray diffraction experiments to 200 GPa with diamond anvil cells. J. Appl. Phys., 101, 123526.

Stretton, I., Heidelbach, F., Mackwell, S. & Langenhorst, F. (2001). Dislocation creep of magnesiowüstite ($Mg_{0.8}Fe_{0.2}O$). Earth Planet. Sci. Lett., 194, 229–240.

Tateno, S., Hirose, K., Ohishi, Y. & Tatsumi, Y. (2010). The structure of iron in Earth's inner core. Science, 330, 359 – 361.

Todd, K. A., Watson, H. C., Yu, T. & Wang, Y. (2016) The effects of shear deformation on planetesimal core segregation: Results from in-situ X-ray micro-tomography. Am. Mineral., 101, 1996-2004

Tommaseo, C. E., Devine, J., Merkel, S., Speziale, S. & Wenk, H.-R. (2006). Texture development and elastic stresses in magnesiowüstite at high pressure. Phys. Chem. Miner., 33, 84–97.

Tromas, C., Girard, J. C. & Woirgard, J. (2000). Study by atomic force microscopy of elementary deformation mechanisms involved in low load indentations in MgO crystals. Philos. Mag. A, 80, 2325–2335.

834 Tsujino, N., Nishihara, Y., Yamazaki, D., Seto, Y., Higo, Y. & Takahashi, E. (2016). Mantle dynamics
835 inferred from the crystallographic preferred orientation of bridgmanite. Nature, 539, 81–84.
836 Turner, P. A. & Tomé, C. N. (1994). A study of residual stresses in zircaloy-2 with rod texture. Acta
837 Metall. Mater., 42, 4143–4153.
838 Uchida, T., Wang, Y., Rivers, M. L. & Sutton, S. R. (2004). Yield strength and strain hardening of MgO
839 up to 8 GPa measured in the deformation-DIA with monochromatic x-ray diffraction. Earth Planet.
840 Sci. Lett., 226, 117–126.
841 Urakawa, S., Terasaki, H. P., Funakoshi, K., Uesugi, K. & Yamamoto, S. (2010) Development of high
842 pressure apparatus for X-ray microtomography at Spring-8. J. Phys.: Conf. Ser., 215, 012026
843 Vinogradov, A., Vasilev, E., Seleznev, M., Máthis, K., Orlov, D. & Merson, D. (2016). On the limits of
844 acoustic emission detectability for twinning. Mater. Lett., 183, 417–419.
845 Wallis, D., Hansen, L. N., Britton, T. B. & Wilkinson, A. J. (2017). Dislocation interactions in olivine
846 revealed by HR-EBSD. J. Geophys. Res. Solid Earth, 122, 7659–7678.
847 Wang, H., Wu, P. D., Tomé, C. N. & Huang, Y. (2010). A finite strain elastic-viscoplastic self-consistent
848 model for polycrystalline materials. J. Mech. Phys. Solids, 58, 594–612.
849 Wang, Y., Duhram, W. B., Getting, I. C. & Weidner, D. J. (2003). The deformation-DIA: A new apparatus
850 for high temperature triaxial deformation to pressures up to 15 GPa. Rev. Sci. Instrum., 74, 3002–
851 3011.
852 Wang, Y. Lesher, C., Fiquet, G., Rivers, M. L., Nishiyama, N., Siebert, J., Roberts, J., Morard, G.,
853 Gaudio, S., Clark, A., Watson, H., Menguy, N. & Guyot, F. (2011). In situ high-pressure and high-
854 temperature X-ray microtomographic imaging during large deformation: A new technique for
855 studying mechanical behavior of multiphase composites. Geosphere, 7, 40-53.
856 Wang, Y., Hilairet, N., Nishiyama, N., Yahata, N., Tsuchiya, T., Morard, G. & Fiquet, G. (2013). High-
857 pressure, high-temperature deformation of $CaGeO_3$ (perovskite)±MgO aggregates: Implications
858 for multiphase rheology of the lower mantle. Geochem. Geophys. Geosyst., 14, 3389–3408.
859 Wang, Y. & Shen, G. (2014). High-pressure experimental studies on geo-liquids using synchrotron
860 radiation a the Advanced Photon Source. J. Earth Sci., 25, 939-958.
861 Wang, Y., Zhu, L., Shi, F., Schubnel, A., Hilairet, N., Yu, T., Rivers, M., Gasc, J., Addad, A., Deldicque,
862 D., Li, Z. & Brunet, F. (2017). A laboratory nanoseismological study on deep-focus earthquake
863 micromechanics. Sci. Adv., 3(7), e1601896.
864 Wehrenberg, C. E., McGonegle, D., Bolme, C., Higginbotham, A., Lazicki, A., Lee, H. J., Nagler, B.,
865 Park, H.-S., Remington, B. A., Rudd, R. E., Sliwa, M., Suggit, M., Swift, D., Tavella, F., Zepeda-
866 Ruiz, L., Wark, J. S. (2017). In situ X-ray diffraction measurement of shock-wave-driven twinning
867 and lattice dynamics. Nature, 550, 496–499
868 Weinberger, M. B., Tolbert, S. H. & Kavner, A. (2008). Osmium metal studied under high pressure and
869 nonhydrostatic stress. Phys. Rev. Lett., 100, 045506.
870 Weiss, J., Lahaie, F. & Grasso, J. R. (2000). Statistical analysis of dislocation dynamics during
871 viscoplastic deformation from acoustic emission. J. Geophys. Res., 105, 433–442.

Wenk, H.-R., Kaercher, P., Kanitpanyacharoen, W., Zepeda-Alarcon, E. & Wang2, Y. (2013). Orientation relations during the α-ω phase transition of zirconium: In situ texture observations at high pressure and temperature. Phys. Rev. Lett., 111, 195701.

Wenk, H.-R., Lonardelli, I., Merkel, S., Miyagi, L., Pehl, J., Speziale, S. & Tommaseo, C. E. (2006). Deformation textures produced in diamond anvil experiments, analysed in radial diffraction geometry. J. Phys.: Condens. Matter, 18, S933–S947.

Wenk, H.-R., Lutterotti, L., Kaercher, P., Kanitpanyacharoen, W., Miyagi, L. & Vasin, R. (2014). Rietveld texture analysis from synchrotron diffraction images. ii. complex multiphase materials and diamond anvil cell experiments. Powder Diffr., 29, 220–232.

Wenk, H.-R., Matthies, S., Donovan, J. & Chateigner, D. (1998). Beartex: a windows-based program system for quantitative texture analysis. J. Appl. Cryst., 31, 262–269.

Wenk, H.-R., Matthies, S., Hemley, R. J., Mao, H. K. & Shu, J. (2000). The plastic deformation of iron at pressures of the Earth's inner core. Nature, 405, 1044–1047.

Xiong, L., Li, B., Tang, Y., Li, Q., Hao, J., Bai, L., Li, X. & Liu, J. (2018). Radial x-ray diffraction study of the static strength and texture of tungsten to 96 GPa. Solid State Commun., 269, 83–89.

Xiong, L., Liu, J., Bai, L., Li, X., Lin, C. & Lin, J.-F. (2014). Strength and structural phase transitions of gadolinium at high pressure from radial x-ray diffraction. J. Appl. Phys., 116, 243503.

Xiong, L., Liu, J., Bai, L., Li, Y., Lin, C., He, D., Peng, F. & Lin, J.-F. (2013). Radial x-ray diffraction of tungsten tetraboride to 86 GPa under nonhydrostatic compression. J. Appl. Phys., 113, 033507.

Xu, Y., Nishihara, Y. & Karato, S. (2005). Development of a rotational drickamer apparatus for large-strain deformation experiments at deep earth conditions. In J. Chen, Y. Wang, T. S. Duffy, G. Shen & L. F. Dobrzhinetskaya (Eds.) Advances in High-Pressure Technology for Geophysical Applications, (pp. 167–182). Amsterdam: Elsevier.

Yamazaki, D. & Karato, S. (2001). High-pressure rotational deformation apparatus to 15 GPa. Rev. Sci. Instrum., 72, 4207–4211.

Yamazaki, D. & Karato, S. (2002). Fabric development in (Mg,Fe)O during large strain, shear deformation: implications for seismic anisotropy in Earth's lower mantle. Phys. Earth Planet. Inter., 131, 251–267.

Yang, W., Huang, X., Harder, R., Clark, J. N., Robinson, I. K. & Mao, H.K. (2013). Coherent diffraction imaging of nanoscale strain evolution in a single crystal under high pressure. Nature Communications, 4(1), 1680.

Yau, A., Cha, W., Kanan, M. W., Stephenson, G. B. & Ulvestad, A. (2017). Bragg coherent diffractive imaging of single-grain defect dynamics in polycrystalline films. Science, 356(6339), 739–742.

Yu, X., Zhang, R., Weldon, D., Vogel, S. C., Zhang, J., Brown, D. W., Wang, Y., Reiche, H. M., Wang, S., Du, S., Jin, C. & Zhao, Y. (2015). High pressure phase-transformation induced texture evolution and strengthening in zirconium metal: Experiment and modeling. Sci. Rep., 5, 12552.

Yu, T., Wang, Y. & Rivers, M. L. (2016) Imaging in 3D under pressure: a decade of high-pressure X-ray microtomography development at GSECARS. Prog. Earth Planet. Sci., 3, 17

28

Yue, B., Hong, F., Merkel, S., Tan, D., Yan, J., Chen, B. & Mao, H.-K. (2016). Deformation behavior across the zircon-scheelite phase transition. 117, 135701.

Zarechnyy, O. M., Levitas, V. I. & Ma, Y. (2012). Coupled plastic flow and phase transformation under compression of materials in a diamond anvil cell: Effects of transformation kinetics and yield strength. J. Appl. Phys, 111, 023518.

Zhang, L., Meng, Y., Yang, W., Wang, L., Mao, W. L., Zeng, Q.-S., Jeong, J. S., Wagner, A. J., Mkhoyan, K. A., Liu, W., Xu, R. & Mao, H.K (2014). Disproportionation of (Mg,Fe)SiO_3 perovskite in Earth's deep lower mantle. Science, 344, 877–882.

Zhou, X., Feng, Z., Zhu, L., Xu, J., Miyagi, L., Dong, H., Sheng, H., Wang, Y., Li, Q., Ma, Y., Zhang, H., Yan, J., Tamura, N., Kunz, M., Lutker, K., Huang, T., Hughes, D. A., Huang, X. & Chen, B. (2020). High-pressure strengthening in ultrafine-grained metals. Nature, 579 (7797), 67-72.

29